THE ASTRONOMICAL JOURNAL VOLUME 112, NUMBER 5 NOVEMBER 1996

CCD PHOTOMETRY AND SPECTROSCOPY OF *IRAS* SOURCES HAVING FAR-IR COLORS SIMILAR TO PLANETARY NEBULAE

B. E. REDDY AND M. PARTHASARATHY

Indian Institute of Astrophysics (IIA), Bangalore 560 034, India
Electronic mail: reddy@iiap.ernet.in, partha@iiap.ernet.in

Received 1996 April 24; revised 1996 July 22

ABSTRACT

CCD imaging and *BVRI* photometry of 14 *IRAS* sources with far-IR colors similar to planetary nebulae and post-AGB stars are presented. Also results of optical and near-IR spectroscopy of 10 of these candidates are given. From the observed flux distribution from 0.4 μm to 100 μm we find the presence of hot dust component in addition to the cold dust component. The stellar temperatures, luminosities and distances are estimated. We also estimated the parameters of the circumstellar dust envelopes. These results suggest that the 14 *IRAS* sources considered here are associated with post-AGB supergiants. © *1996 American Astronomical Society.*

1. INTRODUCTION

Planetary nebulae are strong infrared emitters. The *IRAS* fluxes of planetary nebulae show flux maximum around 25 or 60 μm indicating the presence of detached cold dust shells having temperatures 100 to 300 K. At present 1200 to 1500 planetary nebulae are known. The *IRAS* data may contain a few thousand of these objects which have not yet been identified and studied. Since the evolutionary time from the Asymptotic Giant Branch (AGB) to Planetary Nebula (PN) phase is short, we expect that the remnant of the circumstellar envelope created during the AGB should still be present in a PN. In fact all the transition region objects which are inbetween the tip of the AGB and PNe are expected to have circumstellar dust shells with far-IR colors similar to planetary nebulae. Applying the above mentioned concept many young PNe and post-AGB candidates have been discovered (Parthasarathy & Pottasch 1986, 1989; Habing *et al.* 1987; Pottasch & Parthasarathy 1988; Manchado *et al.* 1989; Preite-Martinez 1988; Garcia Lario *et al.* 1990; and Hu *et al.* 1993a).

In fact Parthasarathy & Pottasch (1986) discovered that some of the high latitude bright F supergiants have dust shells similar to PNe and they concluded that they are low mass stars in post-AGB stage of evolution. Since then several post-AGB objects have been detected from an analysis of *IRAS* data (Parthasarathy & Pottasch 1989; Lamers *et al.* 1986; Waelkens *et al.* 1987; Pottasch & Parthasarathy 1988; Hrivnak *et al.* 1988; Parthasarathy 1993; van der Veen *et al.* 1994). CO observations have also shown that these stars have molecular envelopes with characteristics similar to post-AGB stars (Likkel *et al.* 1987).

In order to ascertain whether an individual *IRAS* source is a post-AGB star or proto-planetary nebula, additional observations are necessary. Optical observations would be useful especially to know their spectral and luminosity class and hence to fix their position in the H-R diagram. As a part of a program to study post-AGB stars and proto-planetary nebulae, we have obtained CCD photometry and low resolution spectra of several *IRAS* sources with far-IR colors similar to PNe. In this paper we present *BVRI* CCD photometry and spectroscopy of 14 *IRAS* sources which are most likely associated with post-AGB stars and proto-planetary nebulae.

2. SAMPLE SELECTION

We have selected the post-AGB stars on the basis of the following criteria:

(a) We have chosen the *IRAS* sources having colors $F_{12}/F_{25} \leq 0.50$ and $F_{25}/F_{60} \geq 0.35$ which are typical of PNe from *IRAS* color-color diagram of Pottasch *et al.* (1990) and objects which have *IRAS* properties inbetween AGB and PNe in the van der Veen & Habing (1988) *IRAS* evolutionary color-color diagram (VH diagram). The positions of these sources are shown in Fig. 1. Three sources are in box IIIb, two are in box IV, five are in box V, and one is in box VIII of the VH diagram. Three sources have very cold dust shells and they fall outside the boundary line ([12]–[25]=2.0) of the VH diagram (Fig. 1). *IRAS* sources in the boxes IIIb, IV, and V in the VH diagram are mostly evolved stars with dust around them. The sources which fall in these boxes are most likely post-AGB stars and planetary nebulae (van der Veen & Habing 1988). The sources in our sample and their corresponding positions in the VH diagram are given in Table 1. (b) We have selected the objects which have good quality *IRAS* fluxes in at least three bands. The 100 μm fluxes which carry "*L*" flag (Table 1) are upper limits and are affected by infrared cirrus (emission from interstellar dust). (c) AGB evolution of low and intermediate mass stars is terminated by loss of the outer hydrogen-rich envelope due to severe mass loss. Severe mass loss will cease when the mass of the hydrogen-rich envelope becomes so small ($\approx 10^{-3}\ M_{\odot}$) that the pulsational amplitude decreases or the pulsation stops altogether (Habing 1990; Schönberner 1990). The average variability of OH/IR stars is around 64% (Likkel 1989). From a study of non-variable OH/IR stars Bedijn (1987) con-

 0004-6256/96/112(5)/2053/11/$10.00

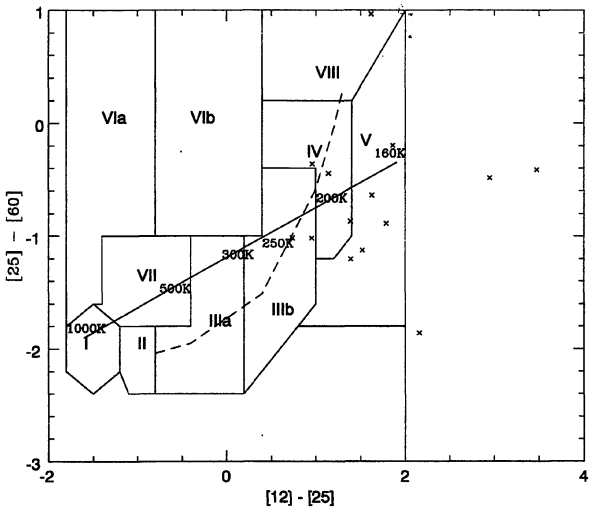

FIG. 1. The positions of program *IRAS* sources in the van der Veen & Habing (1988) *IRAS* color-color diagram. The evolutionary track from Miras to OH/IR stars is indicated by dashed line. The vertical line at [12]–[25]=2 is the boundary line of VH diagram (see text). The sources and their corresponding positions in the VH diagram are given in Table 6.

cluded that they are in the very early post-AGB (transition stage) evolutionary stage. In order to find transition objects, we selected *IRAS* sources with far-IR colors similar to PNe and with very low *IRAS* VAR indices (0 and 1 Ref. *IRAS* PSC and Expl. Suppl 1985). In the *IRAS* PSC the VAR index =(percentage probability source is variable)/10. In the printed version of the *IRAS* PSC the VAR=0 indicates that the percentage probability source is variable is between 0% and 10% and VAR=1 indicates that the percentage probability source is variable is between 10% and 20%. The *IRAS* fluxes and the VAR indices of the selected *IRAS* sources are given in Table 1. (d) We searched for optical associations for the *IRAS* sources having the above criteria on the POSS/ESO optical sky survey plates. We have chosen the objects which have definite optical counterparts. The optical identifications for the sources in our sample are given in Fig. 2. All the sources marked on the CCD frame of *V* filter are stellar in appearance except IRAS 17150−3224 which is a known bipolar PPNe (Hu *et al.* 1993b). In this study we eliminated *IRAS* sources which have spectral features typical of main sequence stars. (e) In order for the sources to be observable from the VBO, Kavalur Observatory we restricted our sample to sources in the declination range +62° to −46° and with optical counterparts brighter than $16^{m}.5$.

3. OBSERVATIONS

3.1 Photometry

We identified the optical counterparts of 14 *IRAS* sources on the POSS and ESO optical sky survey plates. We have obtained *BVRI*, CCD imaging of all these sources using the 1.0 m telescope at the Vainu Bappu Observatory (VBO), Kavalur in 1993 January. Optical photometry has been performed in the Johnson-Cousins system using Thomson CSF Th7882 CCD chip. For calibration we used standards from Landolt (1983) and members of the open cluster M67 from Mayya (1991). The CCD images have been processed using IRAF (Image Reduction and Analysis Facility). Near-IR photometric data have been taken from the literature and far-IR fluxes have been taken from *IRAS* point source catalogue.The results of optical photometry have been tabulated in Table 2.

3.2 Spectroscopy

Low resolution optical spectra of a few bright sources in the sample (Table 1) have been taken during observational runs in 1992 December and 1993 January. We used the 1.0 m telescope at VBO equipped with a UAGS spectrograph and CCD. Spectra from 4000 to 6500 Å with a resolution of 5.7 Å pixel^{-1} were obtained. Low resolution near-IR spectra of several of these sources have also been obtained with the 2.3 m telescope at VBO during 1993 November. We have reduced the spectra using a locally developed software program called RESPECT at VBO Kavalur.

TABLE 1. *IRAS* data of program candidates. VAR is the *IRAS* variability index as given in *IRAS* PSC.

IRAS Name	Association	*IRAS* fluxes (Janskys) 12μ	25μ	60μ	100μ	*l*	*b*	VAR
04296+3429		12.77	45.90	15.12	8.92*L*	166	−09	1
05113+1347		3.79	15.35	5.44	1.62*L*	189	−14	1
05238−0626	BD−06 1178	0.73	1.76	1.26	1.81*L*	209	−22	0
05341+0852		4.52	9.89	3.87	7.77*L*	196	−12	0
06530−0213		6.14	27.45	14.83	03.9	215	−0	0
07253−2001		6.33	15.23	05.95	7.82	235	−01	0
08143−4406		0.61	9.31	5.96	3.64*L*	261	−05	0
08187−1905	HD 70379	0.72	17.69	12.09	3.53	241	10	0
14429−4539		14.68	33.24	13.43	2.81	323	12	1
17086−2403	CD−23 13192	1.61	11.82	2.13	14.89*L*	360	09	0
17150−3224		58.04	321.42	268.29	81.41	354	03	0
17291−2402		2.11	19.33	22.73	11.58	03	05	0
17441−2411	RAFGL 5385	42.86	191.13	106.09	27.54*L*	04	02	0
23304+6147		11.39	59.03	26.38	30.47*L*	114	01	0

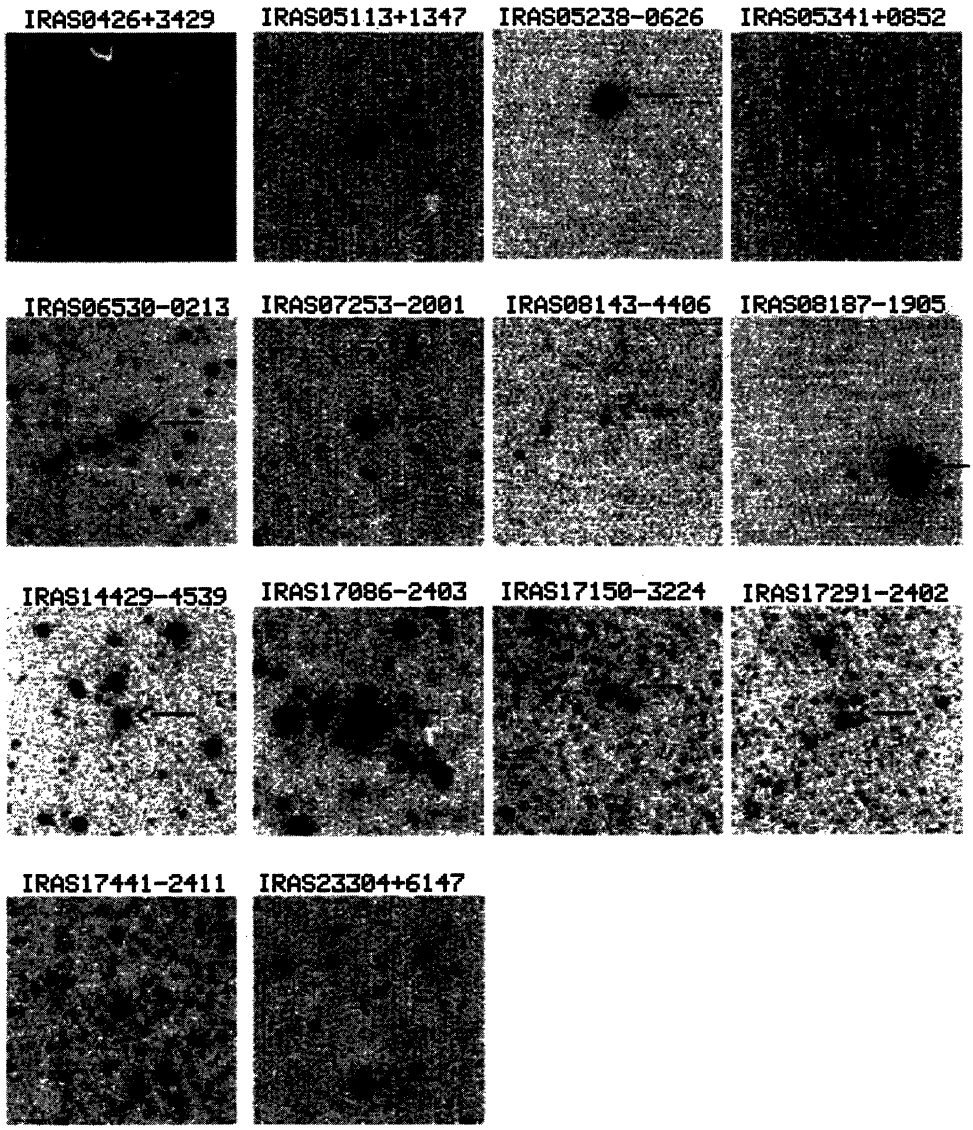

FIG. 2. Optical identification charts of the *IRAS* sources. Identifications are marked on CCD frames of *V* band. The scale of the each figure is 1.5×1.5. For all images North is up and East is left.

4. ANALYSIS

4.1 Spectral Classification

We used both optical and near-IR spectra for spectral classification. In order to compare and classify the objects we obtained spectra of several bright standard stars with the same instrumental setup. We have also used the optical spectra of standard stars compiled by Jacoby *et al.* (1984) for this purpose. The near-IR spectra of program stars have been compared with the spectra of bright standard stars obtained by us and also with the near-IR spectra of several stars given by Torres Dodgen, & Weaver (1993). The near-IR spectral classification agrees well with the optical classification except for IRAS 04296+3429. We classified this star as an F5 supergiant based on the near-IR spectra; Hrivnak (1995) classified it as a G5 supergiant based on the spectrum in the blue region. It is to be noted here that we made use of spectra of normal population I stars to classify the spectra of program stars. Some of the sample stars may be slightly metal poor and therefore spectral types assigned can be a bit earlier. The spectral types and luminosity classes of 8 stars have been reliably estimated and are listed in Table 3. We could get spectra of only 8 stars within the alloted observing time. Several of our program stars are fainter than 13th magnitude and the sky conditions during our observing run were not favourable and hence we ended up with spectra of eight program stars. The optical and NIR spectra of program stars have been displayed in Fig. 3 and Fig. 4 respectively.

4.2 Observed Flux Distribution

The observations of the sources in the various wavelength regions (0.4 μm to 100 μm) were combined to study their energy distributions (Fig. 5). The near-IR photometry of the

TABLE 2. Photometric observations of the program sources.

IRAS Name	*B*	*V*	*R*	*I*	Date of observation.[a]
04296+3429	16.39	14.30	13.10		244,9064.5
	16.20	14.21		11.64	244,7452.5[1]
05113+1347	14.81	12.63	11.46	10.17	244,9006.5
05238−0626	11.04	10.56	10.27	9.91	244,9006.5
	11.01	10.54	10.26	9.97	No date[3]
05341+0852	12.50	11.89	11.47	11.00	244,9006.5
06530−0213	16.23	14.11	12.77	11.46	244,9076.5
	16.43	14.04	12.74	11.40	1989 March[2]
07253−2001	13.79	12.90		11.80	244,9006.5
08143−4406	14.14	12.37	11.65	10.61	244,9005.5
08187−1905	9.53	8.85	8.35	8.09	244,9005.5
14429−4539	14.28	13.49	12.89	12.10	244,9100.5
	14.45	13.39	12.64	12.18	244,9076.5
	14.39	13.54	12.92	12.17	1989 March[2]
17086−2403	12.67	11.80	11.40	11.00	244,9100.5
17150−3224	16.26	14.55	13.55	12.46	244,9064.5
	16.10	14.54	13.60	12.69	1989 March[2]
17291−2402	15.29	14.08	13.40	12.66	244,9076.5
17441−2411	15.06	13.35	12.26	11.21	244,9076.5
23304+6147	15.8	13.5	12.5	10.8	244,9005.5
	15.37	13.06		10.43	244,7452.5[1]
	15.52	13.15	11.79	10.50	244,7762.5[1]

Note: Errors in magnitudes: *B*: ±0.1; *V*,*R*,*I*: ±0.05 1

[1]Hrivnak and Kwok 1991.
[2]Hu *et al.* 1993.
[3]Torres *et al.* 1995.
[a]In Julian date.

sample objects (Table 1) has been taken from the studies of Manchado *et al.* (1989) and Garcia-Lario *et al.* (1990). In order to compare the energy distribution of the program stars with model atmospheres we have to correct the observed fluxes for interstellar reddening. The optical and near-IR fluxes have been corrected for interstellar reddening. We estimated the reddening in the direction of these objects from the work of Burstein & Heiles (1982) and Neckel & Klare (1980). We also estimated interstellar reddening from O- and B-type stars which are in the direction of program stars. We have used both the bright (nearby) and fainter (distant) O and B stars, to minimize the effect of distance on the reddening. The estimated average extinction values A_V have been tabulated in Table 4. Using these values, the *BVRI* and near-IR magnitudes have been corrected for interstellar extinction using the average extinction law of Cardelli *et al.* (1989). The flux distribution of stars are compared with the Kurucz (1979) atmospheric models which are shown in Fig. 5. It is clear from Fig. 5 that all the stars have far-IR excess.

TABLE 3. Spectral types and luminosity classes as derived from optical and near-IR spectra of few sources.

IRAS Name	optical spectrum	NIR spectrum	Date of obs.
IRAS 04296+3429	-	F5I	244,9328.5
IRAS 05113+1347	G3I	G5I	244,8996.5
IRAS 05238−0626	F2II		244,9199.5
IRAS 05341+0852	F6I		244,9199.5
IRAS 06530−0213	-	F0I	244,9328.5
IRAS 07253−2001	-	F5I(e)	244,9199.5
IRAS 08143−4406	F8I	-	244,9199.5
IRAS 08187−1905	F6I	F5I	244,8995.5

4.3 Stellar Temperatures, Gravities, Luminosities and Distances

The effective temperatures and gravities are estimated from the observed energy distribution fits with the Kurucz model atmospheres with solar metallicity. The models were

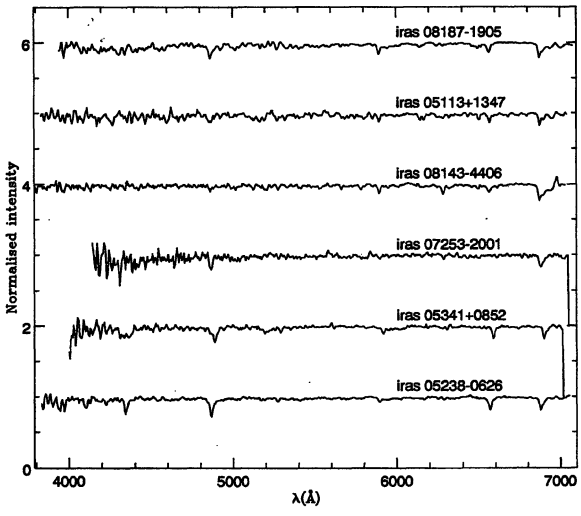

FIG. 3. Normalized low resolution optical spectra of some of the sources.

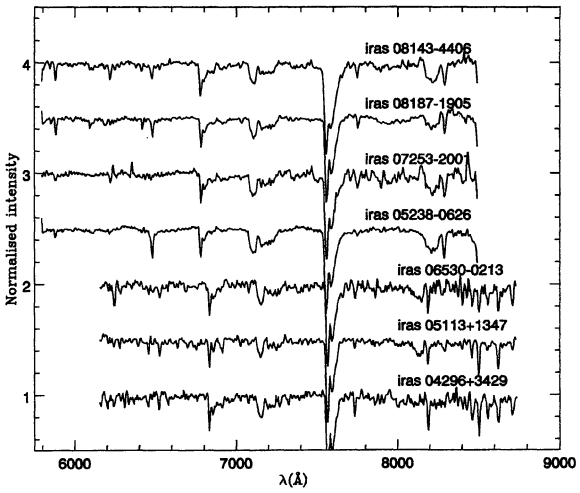

FIG. 4. Normalized low resolution red spectra of few fainter sources.

fitted to three wavelength regions: optical, near-IR and far-IR. The model atmospheres of different metallicities differ considerably only in the UV part of the spectral domain which is sensitive to the metallicity. Since the optical fluxes are from the broad band photometry, and low dispersion spectra of some of these sources do not indicate significant underabundance of metals, we have used Kurucz model atmospheres with solar metallicity. The IR part of the energy distribution is not very sensitive to metallicity. From Fig. 5 it is seen that for several stars, model fits are satisfactory at least in the optical part of the energy distribution. In the case of a few stars (see Fig. 5), large deviations of observed flux distribution from the models may be due to unaccounted interstellar and/or circumstellar reddening.

Since all the stars considered here are *IRAS* sources and have circumstellar envelopes, deducing stellar parameters $T_{\rm eff}$ and $\log g$ from the model fits are largely hampered by the reddening caused by both interstellar medium and circumstellar envelopes. Determination of extinction due to the dust around the stars is difficult as there are no accurate extinction laws which satisfy the dust environment of individual stars. The probable errors $T_{\rm eff}$ and $\log g$ determinations are of the order of ± 500 K and ± 0.5, respectively.

For stars which have spectral types and luminosity classes (Table 3), we estimated temperatures from spectral type vs $T_{\rm eff}$ calibration for supergiants (Flower 1977). Stellar surface gravities are taken from luminosity vs gravity tables. Deriving gravities from the low resolution spectra is difficult, but the supergiant character of the spectra of the sources indicate that they have low-gravity atmospheres. The stellar $T_{\rm eff}$ and $\log g$ values derived from the spectra of IRAS 05238−0626, IRAS 05341+0852, IRAS 07253−2001, IRAS 08187−1905, and IRAS 17086−2403 are in good agreement with the values derived from the model fits. The derived $T_{\rm eff}$ and gravities are presented in Table 4.

Since the distances (d) to these sources are not known, it is difficult to determine the luminosities for these stars. The spectral class vs absolute magnitude tables (Landolt-Börnstein 1982) yield values of $M_V \approx -6.6$ which is very large and valid for the Population I supergiants. The stars considered here all have circumstellar envelopes with far-IR colors typical of post-AGB stars and proto-planetary nebulae. In most of the stars in our sample CO or OH molecular features have been detected which are normally found in the expanding envelopes of evolved low mass stars such as post-AGB stars and proto-planetary nebulae. The summary of molecular observations of these stars is given in Table 6. Since all these sources are post-AGB stars, we assume that they may have a core mass of $M_c \approx 0.6\ M_\odot$. The core mass $M_c = 0.6\ M_\odot$ is typical of observed white dwarfs and central stars of PNe.

The post-AGB stars evolve from the tip of the AGB to planetary nebulae with constant luminosity, but with increasing surface temperature and decreasing radii (Schönberner 1983; Blöcker 1995). The central stars are still burning hydrogen in a thin shell just outside of the stellar core. The stellar envelope mass is still large enough ($M_e > 10^{-4}\ M_\odot$) to ensure that the evolution of the core and envelope are decoupled and the core mass-luminosity relation (Wood and Zaro 1981) is applicable. Using the core mass-luminosity relation, with core mass of $0.6\ M_\odot$ we get stellar luminosity

TABLE 4. Temperatures and fluxes of stars and their dust envelopes.

IRAS Name	$T_{\rm eff}$ (K)	$\log g$	$B-V$	A_v	T_d (K)	$f_{\rm opt}$	$f_{\rm fir}$ $\times 10^{-12}$ W m^{-2}	$f_{\rm ir}/f_{\rm opt}$ $\times 10^{-12}$ W m^{-2}
04296+3429	5500	1.0	2.09	1.6	160	0.137	7.136	50.0
05113+1347	5000	1.0	2.18	0.4	145	0.188	2.36	12.5
05238−0626	7500	1.0	0.48	0.6	143	3.846	0.296	0.08
05341+0852	6500	0.5	0.61	0.4	200	0.804	1.643	2.04
06530−0213	7500	1.0	2.12	1.2	145	0.184	4.269	23.20
07253−2001	7000	1.0	0.89	0.9	210	0.563	2.495	4.43
08143−4406	6000	1.0	1.77	1.2	115	0.651	1.386	2.13
08187−1905	6500	1.0	0.68	0.3	110	11.374	2.614	0.23
14429−4539	5500		0.89	0.6	200	0.213	5.504	25.84
17086−2403	9500	1.0	0.87	1.9	140	3.907	1.701	0.44
17150−3224	5000	1.0	0.87	0.9	150	0.066	50.076	758.7
17291−2402	6000		1.21	0.9	140	0.132	3.076	23.30
17441−2411	9000		1.71	2.8	150	1.555	29.76	19.14
23304+6147	5000	1.0	2.3	2.8	135	0.485	8.99	18.54

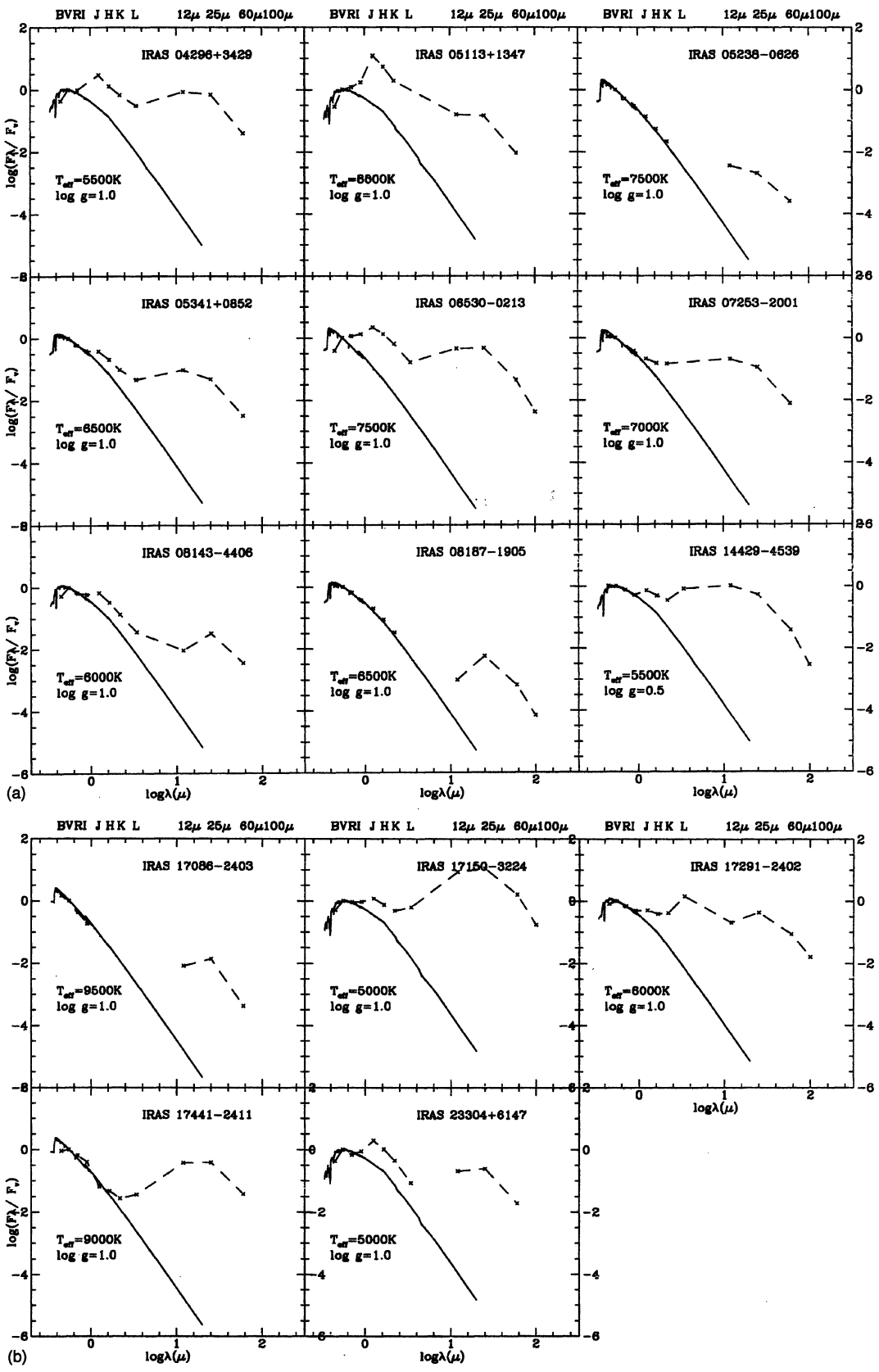

FIG. 5. Spectral energy distribution of program stars showing the presence of both hot and cold dust components. The sources IRAS 05238−0626, IRAS 17086−2403, and IRAS 08187−1905 have only cold dust. The full line indicates the Kurucz model with the parameters given in the figures.

TABLE 5. Derived stellar and dust envelope parameters *IRAS* sources.

IRAS Name	$A_{v\ tot}$	d (kpc)	Z (pc)	$R_\star$ ($R_\odot$)	R_d ($\times 10^5\ R_\odot$)	M_d ($\times 10^4\ M_\odot$)	t_{dyn} (yr)	$M\times 10^{-7}$ $M_\odot$ yr^{-1}
IRAS 04296+3429	3.0	5	0.8	119	2.0	5.9	400	5.1
IRAS 05113+1347	4.3	5	1.2	105	2.6	2.5	550	4.6
IRAS 05233−0626	1.0	7	2.6	47	2.8	1.2	700	2.0
IRAS 05341+0852	0.5	10	2	54	1.1	4.0	300	2.7
IRAS 06530−0213	6.1	3	0.0	43	2.6	2.0	350	1.8
IRAS 07253−2001	2.1	10	0.2	54	1.0	5.7	250	2.0
IRAS 08143−4406	4.0	4	0.4	68	4.8	3.0	1100	3.0
IRAS 08187−1905	1.1	3	0.5	54	5.5	3.9	1300	2.3
IRAS 14429−4539	0.1	6	1.2	87	1.09	5.0	252	3.8
IRAS 17086−2403	3.6	6	1	29	4.1	1.6	800	1.2
IRAS 17150−3224	3.0	<18	0.9	105	2.4	<1545	490	4.6
IRAS 17291−2402	2.0	<23	0.9	73	2.9	<246	642	3.2
IRAS 17441−2411	6.0	2.5	0.1	32	2.4	11	600	1.2
IRAS 23304+6147	4.4	5	87	105	4.9	21	1900	4.5

$L_\star = 10^{3.79}\ L_\odot$. The post-AGB tracks calculated (Blöcker 1995) for the core mass $M_c = 0.6\ M_\odot$ also gives approximately the same luminosity.

The luminosity $\log(L_\star/L_\odot) = 3.79$ corresponds to an absolute magnitude $M_V = -4.75$. The distance estimates by distance modulus method demand knowledge of total extinction caused by dust and the interstellar medium (A_v). Using the A_v values given in Table 4, we arrive at very large values for distances. The presence of dust around these sources makes the stars appear fainter and hence the large distances. To minimize the effect of dust in estimating the distances we proceeded as follows: we determined total excess $E(B-V)$ using observed $(B-V)$ and the intrinsic colors $(B-V)_0$ as derived from the spectra. Since the extinction law for dust shells are not known, we assumed the interstellar extinction law for dust shells also. We applied the extinction constant $R = 3.1$ for both interstellar and dust shells. For stars having both hot and cold dust shells the values of d may be too large especially in the case of IRAS 14429−4539, IRAS 17150 −3224, and IRAS 17291−2402. However, for stars having cold detached dust shells, this approximation gives reasonable distance estimates. The total extinction values $A_{v\ tot}$ used in the distance estimates and derived distances are given in Table 5. The stellar radii are estimated using the relation $L = 4\pi R_\star^2 \sigma T^4$ and the values $R_\star$ are tabulated in Table 5. The uncertainties in the derived stellar radii are subject to the uncertainties in the $T_{\rm eff}$ and the assumed luminosity.

We estimated the total optical fluxes ($f_{\rm opt}$) by integrating the fluxes from 0.34 μm to 0.9 μm and the total far-IR fluxes ($f_{\rm fir}$) by integrating fluxes from 12 μm to 100 μm. The $f_{\rm opt}$, $f_{\rm fir}$, and the ratio $f_{\rm fir}/f_{\rm opt}$ are presented in Table 5. For most of the sources the ratio $f_{\rm fir}/f_{\rm opt} > 1$ suggesting that all these sources are emitting most of their energy in far-IR.

4.4 Dust Envelope Parameters

Temperatures, masses, radii, dynamical ages, and mass loss rates of dust envelopes are estimated as follows:

The dust temperatures (T_d) have been estimated assuming blackbody distribution using the *IRAS* fluxes. We accepted the dust temperature for which the deviation between the observed and calculated fluxes are minimum as judged by χ^2 test. The derived dust temperatures are given in Table 4. The radii of dust envelopes are estimated by equating grain heating by photon absorption with cooling by photon emission. The energy balance equation between the radiation from the star $(4\pi R_\star^2 \sigma T_\star^4)$ and dust envelope $(4\pi R_d^2 \sigma T^4 Q(a,T_d)$ is given by

$$R_\star^2 T_\star^4 = R_d^2 T_d^4 Q(a,T_d), \tag{1}$$

where $Q(a,T_d)$ is an average efficiency of dust emission for a given T_d and dust grain size, $a = 1$ μm. The values of Q ($Q/a \approx 0.13$–$0.5\ \mu{\rm m}^{-1}$) are taken from the calculations of Drain & Lee (1984). Here dust absorption coefficient is taken as 1, with the assumption that total star light is intercepted by dust. However, this assumption may not be true if the dust shell is in the form of a disk.

Dust masses are computed using the formulae given by Barlow (1983) and Hilderbrand (1983) and using the 60 μm flux and the derived T_d

$$M_d = \frac{4a\rho d^2 F_\nu}{3QB_\nu(T_d)}, \tag{2}$$

where ρ is the grain density, d is distance to the source, F_ν is the observed *IRAS* flux, and $B_\nu(T_d)$ is a blackbody function for given dust temperature. We have used $a\rho/Q = 0.013$ gm cm^{-1} which is typical for interstellar dust grains (Drain & Lee 1984). This procedure provides only an estimation for the total mass, since a single temperature and of uniform chemical composition are assumed for grains. The estimated dust envelope masses (Table. 5) are in the range 10^{-3} to $10^{-4}\ M_\odot$ except for IRAS 14429−4539 and IRAS 1715 −3124 which have large dust masses of around $10^{-2}\ M_\odot$.

We next determined the dynamical ages for the post-AGB stars considered here. The dynamical age is the travel time from the dust condensation radius (R_c) to the present radius. We used here the approximate solution of equation of motion for steady radial flow given by van der Veen *et al.* (1989)

TABLE 6. Molecular observations of program stars. VH is the star's position in the van der Veen & Habing (1988) color-color diagram.

IRAS Name	CO	V_{exp}	OH	HCN	3.3μ	21μ	Chem. Type	VH(region)	Ref
05238−0626								IV	
08187−1905								-	
17086−2403	No		No					-	h
04296+3429	Yes	15.6	No	Yes	Yes	Yes	Carbon	V	a,c
05113+1347	...	...	...	...	Yes	Yes	carbon	V	f
05341+0852			No		Yes	Yes	carbon	IIIb	g
06530−0213	Yes	31	No				carbon	IV	b
07253−2001								IIIb	
08143−406								-	
14429−4539	Yes	18.2	No					IIIb	b
17441−2411	Yes		No					V	
23304+6147	Yes	15.5	No	Yes		Yes	carbon	V	a,c
17150−3224	Yes		Yes					V	e
17291−2402								VIII	d

(a) Woodsworth *et al.* 1990; (b) Loup *et al.* 1993; (c) Kwok *et al.* 1989.
(d) Likkel *et al.* 1991; (e) Hu *et al.* 1993b; (f) Hrivnak *et al.* 1994.
(g) Geballe *et al.* 1992; (h) te Lintel Hekkert *et al.* 1991.

$$t_{\rm dyn}=1.73\times10^{3}\left(\frac{L_\star}{5000L_\odot}\right)^{0.5}\left(\frac{T_\star}{10^4\ \rm K}\right)^{0.5}\left(\frac{T_d}{100\ \rm K}\right)^{-2.5}\times\left(\frac{V_\infty}{15\ \rm km\ s^{-1}}\right)^{-1}\ \rm yr. \quad (3)$$

This relation assumes that only radiation pressure and gravity are important and $R_d/R_c>100$ and $T_d<200$ K. The expansion velocities V_∞ are either obtained from the CO or OH observations (see Table 6) or assumed to be equal to 15 km s^{-1}. The estimated values are given in Table 5. The derived results are subject to the uncertainties in the assumed luminosity and derived dust and stellar temperatures. The derived dynamical ages for our sample range from 250 years to 2000 years.

We estimated the present day mass loss rates for the program stars, according to the Reimers (1975) approximated formula:

$$\dot{M}_R=5\times10^{-8}\eta\left(\frac{L_\star}{5000L_\odot}\right)^{1.5}\left(\frac{T_\star}{10^4}\right)^{-2}\left(\frac{M_\star}{M_\odot}\right)^{-1}M_\odot\ \rm yr^{-1}, \quad (4)$$

where η is taken equal to unity and $M_\star=0.6\ M_\odot$. Though Reimers mass loss formula cannot account for the large mass loss rates observed on the AGB ($\approx10^{-4}$ to 10^{-6} $M_\odot$ yr^{-1}), it still gives reasonable mass loss rates for low pulsational period stars (Blöcker 1995). The very low *IRAS* variability index (Table 1) for our program stars justifies the use of this simplified formula. The estimated mass loss values are given in Table 5. All the stars have mass loss rates of the order of 10^{-7} $M_\odot$ yr^{-1}. The uncertainties in the derived mass loss rates are subjected to uncertainties in the assumed luminosity and stellar mass and in the estimated $T_\star$.

5. DISCUSSION

Based on the spectral energy distribution, the sample of program stars are put into two groups. The sources IRAS 08187−1905, IRAS 05238−0626, and IRAS 17086−2403 present similar flux distributions. All three sources have only cold dust components, detached from the central stars with dust radii $R_d\approx1000\ R_\star$. The low infrared variability for all the three sources suggests that these stars have left the AGB. The association of these sources with bright optical candidates, may be due to the thining of the dust envelopes. It may be possible that as the dust shell expands and is diluted, it may lead to higher excitation temperature in the dust because of high effective temperature. At a certain stage the dust shell reaches a level when it cannot sustain the OH and CO molecular emission features. This is consistent with at least one source IRAS 17086−2403, in which OH and CO molecular features are not detected (te Lintel Hekkert *et al.* 1991). Ratag *et al.* (1991) detected 6 cm radio continuum emission in this source which is generally seen in planetary nebulae and proto-planetary nebulae shells. Radio continuum emission is due to thermal bremsstrahlung in a (partially) ionized gas. Radio continuum is detected in very low-excitation PNe (Pottasch *et al.* 1988). Garcia-Lario & Parthasarathy (1996) obtained optical and ultraviolet spectrum of IRAS 17086−2403. They detected nebular emission lines in the optical spectrum indicating that it is a low excitation PN, which is in agreement with the detection of 6 cm radio emission by Ratag *et al.* All three sources are at high galactic latitude ($l>9^0$) suggesting that these are old low-mass evolved stars (Parthasarathy & Pottasch 1986). The *IRAS* colors of these three objects indicate very cold dust shells and all these objects fall out of the range of van der Veen & Habing (VH) (1988) *IRAS* color-color diagram. However in the *IRAS* color-color diagram of Likkel *et al.* (1991) these sources fall in the region where most of the stars are evolved stars and PNe but without CO detection. The far-IR excess, non-variability and high latitude of these objects suggest that these are post-AGB supergiants, slowly evolving towards planetary nebula phase.

The rest of the sources in the sample present a double peak energy distribution (Fig. 5). One peak represents the stellar emission, obscured by optically thin hot dust component and the other is produced by the reemission in the far-IR

of the stellar radiation obscured by the dust envelope. The presence of hot and cold dust components suggest that there was a discontinuity in the mass loss history. A possible cause for such discontinuity may be periodic thermal pulsations predicted for the AGB model stars (Iben & Renzini 1983). The clear separation between maxima, the cool outer dust shell and low IR variability indicate that the dust shell is far away from the central star and the intense mass loss processes are not active now. Observations indicate that the mass loss rates of central stars of planetary nebulae are up to several orders of magnitude below that of the immediately preceding AGB evolution (Perinotto 1989). Therefore, mass loss has to decrease strongly during the transition between the AGB and the PNe. The mass loss values given in Table 5 are almost two orders less than that of the typical mass loss rates of few $\times 10^{-4}$ $M_{\odot}$ yr^{-1} on the AGB phase.

Most of the sources in this second group are classified as carbon-rich based on the infrared properties of their dust envelopes (Omont *et al.* 1993). The carbon-rich dust envelopes imply the overabundance of carbon in the photospheres, which suggest that these stars have undergone third dredge-up which occurs in the advanced phase of AGB evolution of low and intermediate mass stars (Iben & Renzini 1983). Eight out of the eleven sources in this group are identified with having at least one of the molecular carbon features, for example, in IRAS 23304+6147 and IRAS 04296 +3429 CO, HCN and 21 μm emission features are detected (Woodsworth *et al.* 1990 and Loup *et al.* 1993)). The strong unidentified emission feature at 21 μm is not seen in PNe and AGB stars, but only in post-AGB stars (Kwok 1993). In IRAS 17441−2411, IRAS 06530−0213, IRAS 05113 +1347, and IRAS 14429−45389 CO molecular feature has been identified (Omont *et al.* 1993 and references therein). In IRAS 05341+0852 and IRAS 04296+3429 an unidentified 3.3 μm molecular feature has been detected (Geballe and van der Veen 1990) which is generally attributed to Polycyclic Aromatic Hydrocarbons (PAH). In none of these sources OH has been detected. This may be because all these sources are carbon-rich, or the decreased mass loss rate has reduced the OH-density below that required to sustain an OH maser (Sun & Kwok 1987). Lack of OH and low far-IR variability index (Table 1) are consistent with the reduced mass loss (Likkel *et al.* 1991). Most of these sources fall in the region *V* of VH *IRAS* color-color diagram. This region is characterized by stars which are non-variable and perhaps are in the transition phase between AGB and PNe. The carbon-rich dust envelopes and non-variability of these sources suggest that these stars are in the post-AGB stage of evolution.

5.1 Description of Individual Sources

IRAS 04296+3429. This object has been classified as a carbon-rich G0 supergiant using the blue part of the spectrum (Hrivnak 1995). We classified this object as F5 I based on our red spectrum. We use the spectral type derived by Hrivnak, as his spectral resolution is superior to ours. The double peak energy distribution similar to IRAS 06530 −0213 suggests the presence of two dust components, cold and hot. The photometric magnitudes *B* and *V* derived by Hrivnak & Kwok (1991) are in good agreement with our photometric values. The distances 3.6 kpc and 4.2 kpc estimated by Kwok *et al.* (1989) and Omont *et al.* (1993), respectively, are slightly less than the distance 5 kpc derived from our analysis. This may be due to the uncertainties involved in estimating the reddening due to interstellar medium and circumstellar envelope. The characteristics of the dust envelope and the detection of CO, HCN, 3.3 μm and 21 μm (Table 6) emission features indicate that IRAS 04296 +3429 is a carbon-rich post-AGB F-G type supergiant.

IRAS 05113+1347. This is a G type supergiant of magnitude $V = 12.63$. It has large near-IR and far-IR excesses. IRAS 05113+1347 has rising flux at 0.55 μm which reaches peak at 1.25 μm. The large near-IR excess may be due to the thick hot dust component closer to the photosphere of the star. The large value of $E(B - V) = 2.0$ may be due to circumstellar dust. Recently, Hrivnak (1995) has studied the spectra of this source and found strong C2 and C3 absorption features. The large near-IR and far-IR excess, presence of 3.3 μm and 21 μm molecular features (Table 6), the high galactic latitude (−14°) and the spectral type of G3 I suggest that it is carbon-rich post-AGB supergiant similar to IRAS 04296 +3429.

IRAS 05238−0626. This is a high galactic latitude (−21°) F2 supergiant having far-IR excess. The Kurucz model of $T_{\rm eff} = 7500$ K and $\log g = 1.0$ fits very well with the 0.44 μm to 4 μm energy distribution. The $T_{\rm eff} = 8000$ K derived from near-IR fluxes (Garcia *et al.* 1990) agrees with our spectral classification of F2 II. The star has only cold dust component similar to IRAS 08187−1905. The *BVRI* magnitudes derived recently by Torres *et al.* (1995) suggest that there is no variation in the IRAS 05238−0626 brightness (Table 3).

IRAS 05341+0852. This star has an optical counterpart of magnitude $V = 12.63$. This has been classified as F6 supergiant based on both optical and near-IR spectra. The energy distribution of IRAS 05341+0852 has been compared with the Kurucz model of $T_{\rm eff} = 6500$ K and $\log g = 1.0$. The slight deviation of flux distribution from 1 μm to 4 μm from the model fluxes (Fig. 5), suggests that the star has optically thin hot dust component. Geballe and van der Veen (1990) have discovered 3.3 μm emission feature which is generally found in carbon-rich PNs and post-AGB stars (Geballe *et al.* 1992). The presence of 3.3 μm and 21 μm (Table 6) emission features suggest that IRAS 05341+0852 is a carbon-rich post-AGB F supergiant.

IRAS 06530−0213. This source is a F0 supergiant of magnitude $V = 14.11$. Within the uncertainties, our *BVRI* photometry of this source agrees well with the photometry of Hu *et al.* (1993a). We also confirm the spectral class of F0 I estimated by Hu *et al.* The *IRAS* colors place the star in box IV of *IRAS* color-color diagram. The stars in this box are typically stars at the end of their mass loss phase and have very thick oxygen-rich circumstellar shells. The photometry of this object taken in two epochs does not indicate any variability. This object has large reddening $E(B - V) = 1.5$, which might have been affected by unaccountable reddening near the galactic plane as the star is near the plane of the Galaxy. The characteristics of the dust envelope, spectral

type and presence of CO molecular emission suggest it is a post-AGB F supergiant.

IRAS 07253−2001. This star has Hα filled in emission. This source has been classified as F5 supergiant based on its red spectrum. The flux distribution from 0.44 μm to 0.9 μm fits with $T_{\rm eff}$ = 7000 K and log g = 1.0. The shape of the energy distribution from 1 μm to 100 μm (Fig. 5), suggests the presence of warm and cold dust shells. In the van der Veen Habing (1988) *IRAS* color-color diagram this source is in box IIIb which is characterized by stars having increasing mass loss rates.

IRAS 08143−4406. We classify this star as F8 I from its optical spectrum. The energy distribution of IRAS 08143 −4406 indicate that it has optically thin hot dust component in addition to cold dust component similar to IRAS 05341 +0852. This star has been surveyed for radio continuum emission (Van de steen & Pottasch 1993) and is found negative detection.

IRAS 08187−1905. This *IRAS* source is associated with a F6 supergiant of V=8.86. The flux distribution between 0.44 μm and 3.4 μm fits very well with the Kurucz atmospheric model of $T_{\rm eff}$=6500 K and log g=1.0. The $T_{\rm eff}$ = 6300 K derived from the $T_{\rm eff}$ and $V-I$ relation (Jones *et al.* 1995) is in good agreement with the above result. Recently, Garcia *et al.* (1990) from the near-IR photometry indicated that this star may be a main sequence star or a giant. But from our spectra, we classified this object as F6 I. This has been confirmed from our analysis of high resolution spectra. It has very narrow Balmer profiles typical of low gravity stars. The detailed spectroscopic analysis of this candidate will be published elsewhere.

IRAS 14429−4539. This object has been classified as a G0 supergiant by Hu *et al.* (1993a). The flux distribution of this candidate indicates that it has cold and hot dust shells. CO molecular emission has been detected by Nyman *et al.* (1992). The average *BVRI* magnitudes (Table 2) obtained by us are in good agreement with Hu *et al.* (1993a). The estimated distance of the star from its V=13.49 and M_V = −4.7 and E($B-V$) = 0.1 is approximately 35 kpc which is very large. However, Loup *et al.* (1993) infers distance of 6 kpc from molecular observations.

IRAS 17086−2403. This *IRAS* source is associated with an optical candidate of magnitude V = 11.8. The *BVRI* fluxes very well fits with the $T_{\rm eff}$ = 9500 K and log g = 1.0. The $T_{\rm eff}$ = 9500 K corresponds to spectral type of A2. The $V-I$ color of the star after reddening correction corresponds to a temperature of around $T_{\rm eff}$ = 9500 K (Jones *et al.* 1995).

IRAS 17150−3224. This *IRAS* source is a cold bi-polar proto planetary nebula which has been studied by Hu *et al.* (1993b). The *BVRI* photometry of Hu *et al.* (1993a) taken in 1989 agrees with our photometry taken in 1993, showing no evidence for brightness change.

IRAS 17291−2402. This *IRAS* source is associated with an optical candidate of magnitude V=14.08. The shape of the energy distribution from 0.44 μm to 100 μm suggests the existence of a temperature gradient in the circumstellar envelope. From the energy distribution of this star it is clear that star has warm and cold dust components. The CO and OH molecular emissions were not detected (Likkel *et al.* 1991).

IRAS 17441−2411. This *IRAS* source is AFGL 5385. We found its optical position by positional coincidence. Its visual magnitude V = 13.35. The overall flux distribution from 0.44 μm to 100 μm indicates it has large far-IR excess and it has warm and cold dust shells. The *IRAS* colors places it in box IV of VH (1988) diagram. Detection of CO and non-detection of OH molecular emission (Likkel *et al.* 1991) indicates that the star may have a carbon-rich circumstellar envelope. According to the far-IR colors, this star falls in the region (Likkel *et al.* 1991) of *IRAS* color-color diagram of very cold objects, where PPNe and evolved stars with CO detection are present. The observed $B-V$ = 1.7, and E($B-V$) = 0.9 yields the $B-V$ = 0.8 which corresponds to spectral type not later than G0. We conclude that IRAS 17441−2411 is a post-AGB star.

IRAS 23304+6147. This object appears to be similar to IRAS 04296+3429. The presence of CO molecular emission and 21 μm emission (Woodsworth *et al.* 1990; Kwok *et al.* 1989) indicate that it has a carbon-rich circumstellar envelope. The CCD *BVRI* images of this star are stellar in appearance. The *BVRI* magnitudes obtained by us and those obtained by Hrivnak & Kwok (1991) are given in Table 2. The *BVRI* magnitudes obtained at three different epochs, suggest that IRAS 23304+6147 is gradually becoming fainter. But there is no significant variation in ($B-V$). The distance d = 4 kpc inferred from molecular observations (Omont *et al.* 1993) is comparable to the distance d = 5 kpc derived in the present work.

6. CONCLUSIONS

We studied 14 *IRAS* sources with far-IR colors similar to PNe and post-AGB stars. We compared energy distributions of these sources with Kurucz atmospheric models and found that most of the sources have both hot and cold dust components. The sources IRAS 05238−0626, IRAS 08187−1905, and IRAS 17086−2403 have only cold dust components. From low resolution optical spectra and *BVRI* photometry we derived spectral types and luminosity classes for these sources. We estimated the stellar and dust envelope parameters of these stars. The dust envelope characteristics, low infrared flux variability, high galactic latitude, spectral type and supergiant luminosity class suggest that these 14 *IRAS* sources with far-IR (*IRAS*) colors similar to planetary nebulae are post-AGB stars. The dust envelopes around these stars are the result of severe mass loss experienced by these during their AGB stage of evolution. None of these sources are associated with star forming regions. Several of these sources have CO molecular envelopes with expansion velocities similar to those of evolved stars. Our sample also contains sources showing 3.3 μm and 21 μm emission features indicating that these are carbon-rich post-AGB stars.

We thank Professor R. L Kurucz for providing grid of model atmospheres. This research has made use of the SIMBAD data base, operated at CDS, Strasbourg, France. We thank the referee for his valuable comments.

REFERENCES

Bedijn, P. J. 1987, A&A, 186, 136
Blöcker, T. 1995, A&A, 299, 755
Burstein, D., & Heiles, C. 1982, AJ, 87, 1172
Cardelli, J. A., Clayton, G. C., & Mathis, J.s. 1989, ApJ, 345, 245
Draine, B. T., & Lee, H. M. 1984, ApJ, 285, 89
Flower, P. J. 1977, A&A, 54, 31
Garcia-Lario, P., Manchado, A., Pottasch, S. R., Suso, J., & Olling, R. 1990, A&AS, 82, 497
Garcia-Lario, P., & Parthasarathy, M. 1996 (in preparation).
Geballe, T. R., Tielens, A. G. G. M., Kwok, S., & Hrivnak, B. J. 1992, ApJ, 387, L89
Geballe, T. R. & van der Veen, W. E. c. J. 1990, A&A, 235, L9
Habing, H. J., van der Veen, W. E. C. J., & Geballe, T. 1987, in Late stages of Stellar evolution, edited by S. Kwok and S. R. Pottasch (Reidel, Dordrecht), p. 91
Habing, H. J. 1990, in From Miras to Planetary Nebulae, edited by M. O. Mennessier and A. Omont (Editions Frontiers, Gif sur Yvette), p. 16
Hilderbrand, R. H. 1983, QJRAS, 24, 267
Hrivnak, B. J. 1995, ApJ, 438,341
Hrivnak, B. J., Kwok, S., & Volk, K. 1988, ApJ, 331, 832
Hrivnak, B. J., & Kwok, S. 1991, ApJ, 368, 564
Hrivnak, B. J., Kwok S., & Geballe, T. R. 1994, ApJ, 420, 783
Hu, J. Y., Slijkuis, S., de Jong, T., & Jiang, B. W. 1993a, A&AS, 100, 413
Hu, J. Y., Slijkuis, S., Ngugen-Q-Reiu, & de Jong, T. 1993b, A&A, 273, 185
Iben, Jr., I, & Renzini, A. 1983, ARA&A, 21, 271
Jacoby, G. H., Hunter, D. A., & Christian, C.A. 1984, ApJS, 56, 257
Jones, J. B., Wyse, R. F. G., & Gilmore, G. 1995, PASP, 107, 632
Kurucz, R. L. 1979, ApJS, 40, 1
Kwok, S., Volk, K. M., & Hrivnak, B. J. 1989, ApJ, 345, L51
Kwok, S. 1993, ARA&A, 31, 63
Lamers, H. J. G. L. M., Waters, L. B. F. M., Garmany, C. D., Perez, M. R., & Waelkens, C. 1986, A&A, 154, L20
Landolt, A. 1983, ApJ, 88, 439
Likkel, L., Morris, M., Omont, R., & Forveille, T. 1987, A&A, 173, 11
Likkel, L. 1989, ApJ, 344, 350
Likkel, L., Forveille, T., Omont, A., & Morris, M. 1991, A&A, 246, 153
Loup, C., Forveille, T., Omont, A., & Paul, J. F. 1993, A&AS, 99, 291
Manchado, A., Pottasch, S. R., Garcia-Lario, P., Esteban, C., & Mampaso, A. 1989, A&A, 214,139
Mayya, Y. D. 1991, JAA, 12,319
Neckel, Th., & Klare, G. 1980, A&AS, 42, 251
Nyman, L. A., *et al.* 1992, A&AS, 93, 121
Omont, A., Loup, C., Forveille, T., te Lintel Hekkert, P., Habing, H., & Sivagnanam, P. 1993, A&A, 267, 515
Parthasarathy, M., & Pottasch, S. R. 1986, A&A, 154, L16
Parthasarathy, M., & Pottasch, S. R. 1989, A&A, 225, 521
Parthasarathy, M. 1993, ApJ, 414, L109
Perinotto, M. 1989, in Planetary Nebulae, IAU Symp. No 131, edited by S. Torres-Peimbert (Reidel, Dordrecht), p. 293
Pottasch, S. R., & Parthasarathy, M. 1988, A&A, 192, 182
Pottasch, S. R. 1987, Planetary Nebulae (Reidel, Dordrecht)
Pottasch, S. R. *et al.* 1988, A&A, 205, 248
Pottasch, S. R., Ratag, M. A., & Olling, R. 1990, in From Miras to Planetary Nebulae, edited by M. O. Mennessier and A. Omont (Editions Frontiers, Gif sur Yvette, France), p. 381
Preite-Martinez, A. 1988, A&AS, 76, 317
Ratag, M. A., Pottasch, S. R. 1991, A&AS, 91, 481
Reimers, D. 1975, in Problems in Stellar Atmospheres and Envelopes, edited by B. Baschek *et al.* (Springer, Berlin), p. 229
Schönberner, D. 1983, ApJ, 272, 708
Schönberner, D. 1990, in From Miras to Planetary Nebulae, edited by M. O. Mennessier and A. Omont (Editions Frontiers, Gif sur Yvette, France), p. 355
Sun, J., & Kwok, S., 1987, A&A, 185, 258
te Lintel Hekkert, p., Caswell, J. L., Habing, H. J., Haynes, R.F., & Norris, R. P. 1991, A&AS, 90, 327
Torres Dodgen, Ana A., & Weaver, Wm. B. 1993, PASP, 105, 693
Torres, C. A. O., Quast, G., de la Reza, R., Gregorio-Hetem, J., & Lepine, J. R. D. 1995, AJ, 109, 2146
van der Veen, W. E. C. J., & Habing, H. J. 1988, A&A, 194, 125
van der Veen, W. E. C. J., Habing, H. J., & Geballe, T. R. 1989, A&A, 226, 108
van der Veen, W. E. C. J., Waters, L. B. F. M., Trams, N. R., & Matthews, H. E. 1994, A&A, 285, 551
Van de Steene, G. C. M., & Pottasch, S. R. 1993, A&A, 274, 895
Waelkens, C., Waters, L. B. F. M., Cassatella, A., Le Bertre, T., & Lamers, H. J. G. L. M. 1987, A&A, 181, L5
Wood, P. R., & Zaro, D. M. 1981, ApJ, 247, 247
Woodsworth, A. W., Kwok S., and Chen, S. J. 1990, A&A, 228, 503

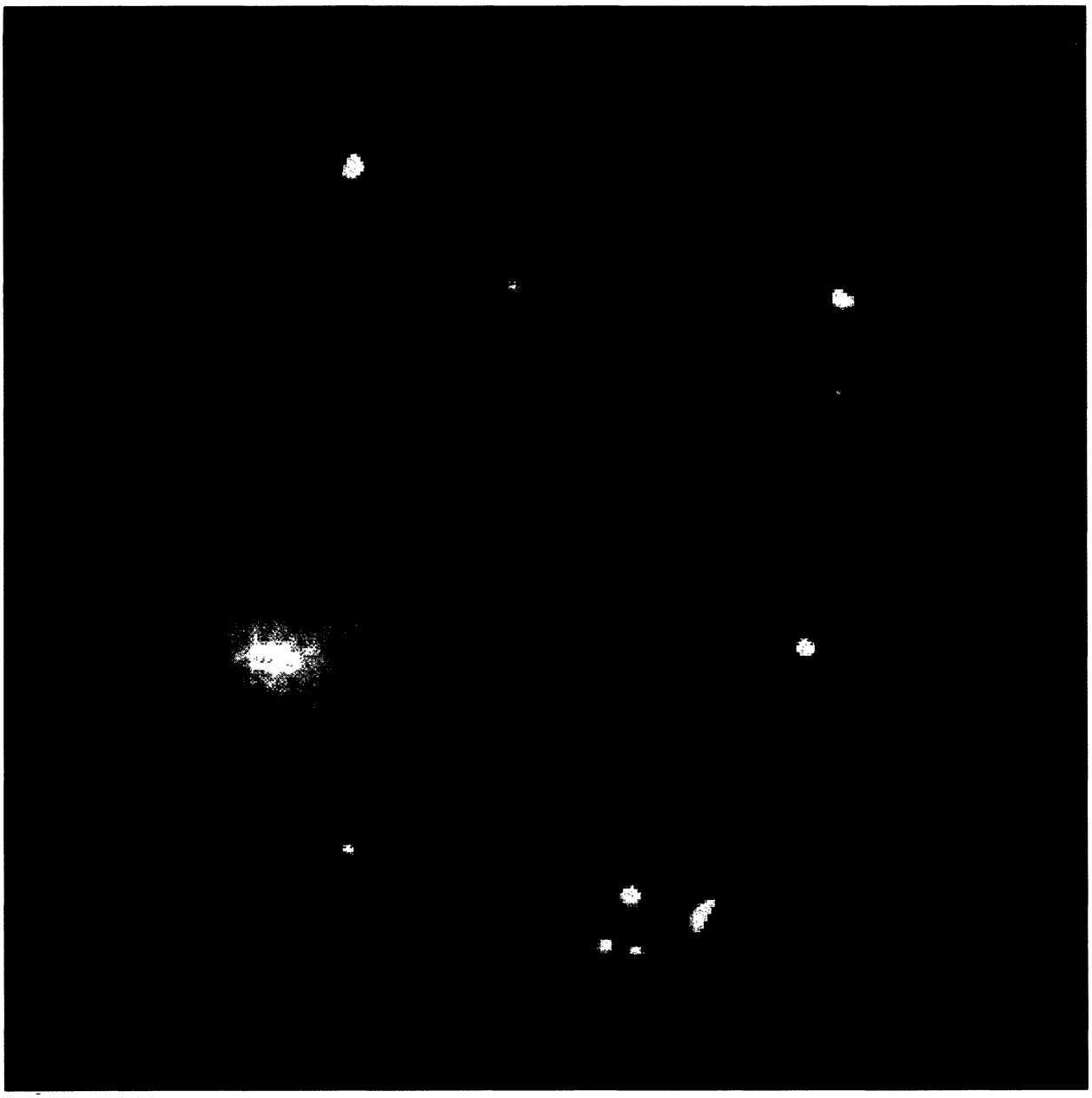

FIG. 6. Composite color image of IRAS 04368+2557 made from the *JHK* surface brightness images. Red=*K*, green=*H*, and blue=*J*. Note the bipolar structure of the IR nebula and its large change of color toward the east away from the central "dark lane." North is top and east is left. The field of view of this image is 201″×201″. The cross indicates the position of the millimeter continuum source (Ohashi *et al.* 1996a).

Tamura *et al.* (see page 2082)